# Turbulent kinetic dissipation analysis for residual-based large eddy simulation of incompressible turbulent flow by variational multiscale method

Chen, Linfeng; Hulshoff, Steven J.; Dong, Yuhong

**DOI**
10.1016/j.cma.2021.114280

**Publication date**
2022

**Document Version**
Final published version

**Published in**
Computer Methods in Applied Mechanics and Engineering

Available online at www.sciencedirect.com
ScienceDirect
Comput. Methods Appl. Mech. Engrg. 388 (2022) 114280
Computer methods in applied mechanics and engineering
www.elsevier.com/locate/cma

# Turbulent kinetic dissipation analysis for residual-based large eddy simulation of incompressible turbulent flow by variational multiscale method

Linfeng Chen[a,*], Steven J. Hulshoff[b], Yuhong Dong[c,d,e]

[a] School of Naval Architecture and Ocean Engineering, Jiangsu University of Science and Technology, Zhenjiang 212100, China
[b] Faculty of Aerospace Engineering, Delft University of Technology, Kluyverweg 1, 2629 HS Delft, The Netherlands
[c] School of Mechanics and Engineering Science, Shanghai University, Shanghai 200072, China
[d] Shanghai Institute of Applied Mathematics and Mechanics, Shanghai 200072, China
[e] Shanghai Key Laboratory of Mechanics in Energy Engineering, Shanghai 200072, China

Received 22 April 2021; received in revised form 31 August 2021; accepted 16 October 2021
Available online xxxx

**Abstract**

The underlying physical mechanism of the residual-based large eddy simulation (LES) based on the variational multiscale (VMS) method is clarified. Resolved large-scale energy transportation equation is mathematically derived for turbulent kinetic energy budget analysis. Firstly, statistical results of benchmark turbulent channel flow at $Re_\tau = 180$ obtained using a coarse mesh are compared with the results obtained by the classical LES with the Smagorinsky and dynamic subgrid stress (SGS) model. The present LES shows an advantage in predicting the statistical results of the incompressible turbulent flows. Secondly, the contributions of the unresolved small-scale presentation terms (Term I-IV in Eq. (10)) to the turbulent kinetic dissipation are analysed for the VMS method. The results show that the turbulent kinetic dissipation provided by the numerical diffusion in the VMS method is smaller in the inner layer, larger in the outer layer of the channel flow than those by the Smagorinsky and dynamic SGS model. The turbulent kinetic dissipation in the VMS method is mainly given by the numerical diffusion provided by one of the "cross-stress" terms (Term I, same as the stabilization term in the SUPG method) and LSIC term (Term IV). The other one of the "cross-stress" terms (Term II) gives rise to the positive turbulent kinetic energy budget, and does not dissipate the turbulent kinetic energy. The so-called "Reynolds stress" term (Term III) dissipates the turbulent energy but provides a very small numerical diffusion. Finally, on the basis of the turbulent kinetic energy dissipation analysis, a new residual-based stabilized finite element formulation is proposed by modifying the large-scale equation in the VMS method. Numerical experiments of 2D lid-driven cavity flow and 3D incompressible turbulent channel flow are tested to validate the proposed formulation. It is shown that all the stabilization terms in the proposed formulation produce additional numerical diffusions and physically increase the total turbulent kinetic dissipation. Consequently, an apparent improvement in both the first-order and second-order statistical quantities are pursued by the new stabilized finite element formulation.


*Keywords:* Residual-based large eddy simulation; Variational multiscale method; Large-scale energy transportation; Turbulent kinetic dissipation; New stabilized finite element formulation

* Corresponding author.
*E-mail address:* chen.linfeng@hotmail.com (L. Chen).

https://doi.org/10.1016/j.cma.2021.114280
0045-7825/

## 1. Introduction

A new LES-type variational multiscale (VMS) theory was presented by Calo [1] and Bazilevs [2] for turbulent simulations. Its basic idea is to perform scale separation for solutions to the Navier–Stokes equations (dividing the solutions into resolved large and unresolved small scales) and to use variational projections for the different scale levels in place of the traditional filtered equations [3]. The approach pays efforts to find an approximate analytical modelling for the unresolved small scales and allows to only solve the resolved large-scale equations accounting to the effect of the unresolved small scales by introducing their approximate analytical modelling [4]. By means of the scale separation in finite element spaces, the effect of the unresolved small scales on the resolved large-scale equations can be approximated in different ways, leading to different closure models (subscale models). In all cases these models are driven by the residual of the Navier–Stokes equation for the resolved large scales in its original form, thus the approach is called residual-based large eddy simulation (LES) [5].

The classical LES technique uses a physical (functional or structural) model to model the extra term caused by the filtering of Navier–Stokes equations and is usually referred to as explicit LES [6]. By contrast, the unresolved small-scale model in the residual-based LES is an addition of purely dissipative numerical terms and no eddy viscosity is introduced. Therefore, it can be categorized as implicit LES (ILES). Derived from the variational multiscale method, the residual-based LES not only permits the use of equal-order interpolation for the velocity and pressure but also precludes global nonphysical oscillations encountered in the convection-dominated problems [4,7]. In contrast with the classical LES based on filtering, the modelling confined to the unresolved small-scale equations in the residual-based LES retains numerical consistency in the resolved large-scale equations and permits full rate of convergence of the underlying numerical method [2], whereas, e.g. the convergence rate of the classical LES is limited to $O(h^{4/3})$ due to the artificial viscosity effects in the resolved large scales [8,9]. Furthermore, avoidance of filters in this approach precludes certain difficulties encountered in the traditional approach, e.g. inhomogeneous non-commutative filters necessary for wall-bounded flows, use of complex filtered quantities in compressible flows.

Holding the promise of much more accurate and efficient LES procedures, the residual-based variational multiscale model has already demonstrated its viability and practical utility [10,11]. By using isogeometric analysis for the space approximation (non-uniform rational B-splines, NURBS [12]), excellent results of forced isotropic turbulence, turbulent channel flow and flow in a planar asymmetric diffuser were presented by Bazilevs et al. [2,13]. Application to the computation of rotating Taylor–Couette flow at high Reynolds number was also performed and it was found that the residual-based modelling is important for conserving angular momentum in the flows dominated by rotation [14]. The approach was successfully applied to studies on concentric pipe flows [15], coupled multi-ion transport in dilute electrolyte solutions [16], nonequilibrium plasma flows [17], bingham flows [18] and boundary shear flows past subsea pipeline [19–21]. On the basis of this approach, new models for many more complicated problems were also further proposed, e.g. the models for premixed combustion problem [22], multiphase flows with surface tension [23–25], fluid–structure interaction in the free-surface flows [26–31] and stratified turbulent flows [32].

On the other hand, many efforts were also paid to assessment of the variational multiscale model for the large eddy simulations. Akkerman et al. [33] examined the role of continuity of the basis in the computation of turbulent flows and found that the smooth NURBS basis functions had advantages over standard finite elements. A spectral analysis for the dissipation of the residual-based multiscale method was presented by Wang and Oberai [34], and the dissipation of the model terms was provided under restrictive conditions, which however leads to the only use of spectral methods. Principe et al. [35] presented the dissipative structures for a surface-mounted obstacle problem and revealed that the numerical dissipation introduced by the residual-based small-scale model is of the same order as the subgrid dissipation by the Smagorinsky model. Colomes et al. [36] examined different unresolved small-scale approximations (including either static or dynamic subscales), linear or nonlinear multiscale splitting and different choices of the subscale space for the residual-based LES. They concluded that the numerical results obtained by the different VMS formulations (as far as they converge) are quite similar. Eikelder and Akkerman [37] introduced orthogonal unresolved small scales to create a link among VMS, SUPG (streamline-upwind Petrov–Galerkin method) and GLS (Galerkin/least-squares method) and proposed two stabilized finite element methods (a novel GLS method with dynamic unresolved small-scale model) to rectify the energy evolution for the incompressible Navier–Stokes equations [38]. Numerical assessments of the residual-based and projection-based variational multiscale methods were performed by Ahmed and John [39,40]. It was concluded that the residual-based VMS and SUPG method gave more accurate results than the projection-based VMS method.

Although certain assessments of the residual-based LES have been made, physical understanding for the variational multiscale model has not been pursued yet. Ahmed and John mentioned that the residual-based VMS method does not show an advantage in contrast to the SUPG method. However, no physical elaboration was given for such a statement. The present study is devoted to a derivation of the resolved large-scale energy transportation equation and estimations of the numerical dissipations of the static unresolved small-scale model terms for the VMS method. In the first stage of the study, analyses of the statistical dissipation of each model term along the wall-normal direction in a benchmark turbulent channel flow are performed so as to physically clarify the role of each model term for the residual-based LES. In the second stage, on the basis of the dissipation analyses for the VMS method, a new residual-based stabilized finite element formulation is proposed for large eddy simulation by modifying the resolved large-scale equation in the VMS method. Numerical experiments of 2D lid driven cavity flow and 3D incompressible turbulent channel flow are performed to validate the proposed formulation.

## 2. Mathematical model for residual-based ILES

### 2.1. Strong form of incompressible Navier–Stokes equations

Considering the flow in a spatial domain $\Omega \subset R^d$ with a piecewise smooth boundary $\Gamma = \partial\Omega$, the incompressible Navier–Stokes equations governing the fluid flow in a strong form are stated as

$$\nabla \cdot \boldsymbol{u} = 0, \tag{1}$$

$$\frac{\partial \boldsymbol{u}}{\partial t} + (\boldsymbol{u} \cdot \nabla)\boldsymbol{u} + \nabla p - \nabla \cdot (2\nu \nabla^s \boldsymbol{u}) = \boldsymbol{f}, \tag{2}$$

where $\boldsymbol{u} : Q \to R^d$ denotes a vector of the velocity and $p : Q \to R$ represents the pressure divided by the density, with $Q = \Omega \times (0, T)$, $\nu$ is the kinematic viscosity, $\boldsymbol{f}$ is the body force (per unit volume). $\nabla^s \boldsymbol{u} = (\nabla \boldsymbol{u} + (\nabla \boldsymbol{u})^T)/2$.

### 2.2. Weak formulations

To derive the weak formulations of Eqs. (1) and (2), we denote the trial-solution and weighting function space, which belong to the same function space by adopting homogeneous initial and boundary conditions, by $\mathcal{S}$. Denoting the weighting functions by $\boldsymbol{W} = \{\boldsymbol{w}, q\}$, the trial solutions by $\boldsymbol{U} = \{\boldsymbol{u}, p\}$, multiplying Eqs. (1) and (2) by $\boldsymbol{W} = \{\boldsymbol{w}, q\}$ and performing their integrations over the discrete element domain yields their standard Galerkin formulations

$$B(\boldsymbol{W}, \boldsymbol{U}) = (\boldsymbol{W}, \boldsymbol{F}) \tag{3}$$

where

$$\begin{aligned} B(\boldsymbol{W}, \boldsymbol{U}) = &\left(\boldsymbol{w}, \frac{\partial \boldsymbol{u}}{\partial t}\right)_\Omega + (\boldsymbol{w}, \boldsymbol{u} \cdot \nabla \boldsymbol{u})_\Omega + (\boldsymbol{w}, \nabla p)_\Omega \\ &- \left(\boldsymbol{w}, \nabla \cdot (2\nu \nabla^s \boldsymbol{u})\right)_\Omega + (q, \nabla \cdot \boldsymbol{u})_\Omega, \end{aligned} \tag{4}$$

and $\boldsymbol{F} = \{\boldsymbol{f}, 0\}$, $(\cdot, \cdot)_\Omega$ is used for a denotation of inner product integration in the discrete element domain. This formulation implies weak satisfaction of the incompressibility constraint and the momentum equation.

### 2.3. Variational multiscale formulations

The variational multiscale method introduces scale decomposition and replaces the traditional filter in LES with variational projection for the different scale levels. By virtue of the variational multiscale theory, the weighting function spaces and the function spaces of trial solutions can be divided into a "resolved large-scale" component and a "unresolved small-scale" component respectively [4,7],

$$\boldsymbol{W} = \boldsymbol{W}^h + \boldsymbol{W}', \tag{5}$$

$$\boldsymbol{U} = \boldsymbol{U}^h + \boldsymbol{U}', \tag{6}$$

Eq. (3) can then be split into two coupled nonlinear subsystems

$$B(\boldsymbol{W}^h, \boldsymbol{U}^h + \boldsymbol{U}') = (\boldsymbol{W}^h, \boldsymbol{F}), \tag{7}$$

$$B(\boldsymbol{W}', \boldsymbol{U}^h + \boldsymbol{U}') = (\boldsymbol{W}', \boldsymbol{F}), \tag{8}$$

where Eqs. (7) and (8) are named as resolved large- and unresolved small-scale equations respectively. The resolved large-scale equations, defined in a finite-dimensional space, are to be numerically solved. However, the unresolved small-scale equations which are defined in the left space are not to be solved but used for a derivation of approximate expression of the small scales. Eq. (7) can be expanded to

$$\begin{aligned} B(\boldsymbol{W}^h, \boldsymbol{U}^h + \boldsymbol{U}') = {} & B(\boldsymbol{W}^h, \boldsymbol{U}^h) \\ & + \left(\boldsymbol{w}^h, \frac{\partial \boldsymbol{u}'}{\partial t}\right)_\Omega - \left(\boldsymbol{w}^h, 2\nu\nabla\cdot(\nabla^s \boldsymbol{u}')\right)_\Omega \\ & + (\boldsymbol{w}^h, \nabla p')_\Omega \\ & + (\boldsymbol{w}^h, \boldsymbol{u}'\cdot\nabla\boldsymbol{u}^h)_\Omega + (\boldsymbol{w}^h, (\boldsymbol{u}^h + \boldsymbol{u}')\cdot\nabla\boldsymbol{u}')_\Omega \\ & + (q^h, \nabla\cdot\boldsymbol{u}')_\Omega = (\boldsymbol{w}^h, \boldsymbol{f})_\Omega. \end{aligned} \tag{9}$$

By a treatment used in [20,33][?], Eq. (9) is simplified as

$$\begin{aligned} & \left(\boldsymbol{w}^h, \frac{\partial \boldsymbol{u}^h}{\partial t}\right)_\Omega + (\boldsymbol{w}^h, \boldsymbol{u}^h\cdot\nabla\boldsymbol{u}^h)_\Omega - (\nabla\boldsymbol{w}^h, p^h)_\Omega + \left(\nabla^s\boldsymbol{w}^h, 2\nu\nabla^s\boldsymbol{u}^h\right)_\Omega + (q^h, \nabla\cdot\boldsymbol{u}^h)_\Omega \\ & \underbrace{-\sum_{e=1}^{n_{el}}\left(\nabla\boldsymbol{w}^h, \boldsymbol{u}^h\otimes\boldsymbol{u}'\right)_{\Omega_e}}_{\mathrm{I}} \underbrace{+\sum_{e=1}^{n_{el}}\left(\boldsymbol{w}^h, \boldsymbol{u}'\cdot\nabla\boldsymbol{u}^h\right)_{\Omega_e}}_{\mathrm{II}} \underbrace{-\sum_{e=1}^{n_{el}}\left(\nabla\boldsymbol{w}^h, \boldsymbol{u}'\otimes\boldsymbol{u}'\right)_{\Omega_e}}_{\mathrm{III}} \\ & \underbrace{-\sum_{e=1}^{n_{el}}\left(\nabla\cdot\boldsymbol{w}^h, p'\right)_{\Omega_e}}_{\mathrm{IV}} \\ & \underbrace{-\sum_{e=1}^{n_{el}}\left(\nabla q^h, \boldsymbol{u}'\right)_{\Omega_e}}_{\mathrm{V}} \\ & + \sum_{e=1}^{n_{eb}}\left(\boldsymbol{w}^h, p^h\boldsymbol{n} - 2\nu\nabla^s\boldsymbol{u}^h\cdot\boldsymbol{n}\right)_{\Gamma_e} \\ & = (\boldsymbol{w}^h, \boldsymbol{f})_\Omega, \end{aligned} \tag{10}$$

where $\boldsymbol{u}^h\otimes\boldsymbol{u}' = u_j^h u_i'$, $\Gamma$ denotes the boundaries of the computational domain, and $\boldsymbol{n}$ represents the outward normal vector to the boundary.

In Eq. (10), the second, third and fourth lines on the left-hand side represent consistent unresolved small-scale representations. With an introduction of algebraic approximation of the small scales, these terms depend explicitly on the large scales and are analogic to the SGS model in the classical LES. In this context no assumption about the effect of the small scales on the represented ones is introduced nor is an eddy viscosity required. For the unresolved small-scale terms arising from the nonlinear splitting (the second line) in Eq. (10), Bazilevs and Calo interpreted that $(\boldsymbol{w}^h, \boldsymbol{u}'\cdot\nabla\boldsymbol{u}^h)_\Omega - (\nabla\boldsymbol{w}^h, \boldsymbol{u}'\otimes\boldsymbol{u}^h)_\Omega$ was an analog of the Cross stress term in the Subgrid-scale stress, and $-(\nabla\boldsymbol{w}^h, \boldsymbol{u}'\otimes\boldsymbol{u}')_\Omega$ corresponds to the Reynolds stress term. Their practical contributions will be clarified in the later discussions. The fifth line in Eq. (10) is yielded by integration by parts.

Based on the unresolved small-scale equations, $\boldsymbol{u}'$ and $p'$ can be approximated as [7,41,42]

$$\boldsymbol{u}' = -\tau_m \boldsymbol{r}_m, \tag{11}$$

$$p' = -\tau_c r_c, \tag{12}$$

where $\boldsymbol{r}_m$ and $r_c$ respectively represent the residual of Eq. (2) and (1) associated with $\{\boldsymbol{u}^h, p^h\}$, $\boldsymbol{\tau}_m$ and $\tau_c$ are defined as follows [43,44]

$$\tau_m = \left(c_1 \boldsymbol{u}^h \boldsymbol{G} \boldsymbol{u}^h + c_2 \nu^2 \boldsymbol{G} : \boldsymbol{G} + \frac{c_3}{\Delta t^2}\right)^{-\frac{1}{2}} \tag{13}$$

$$\tau_c = \frac{\boldsymbol{u}^h \boldsymbol{G} \boldsymbol{u}^h}{tr(\boldsymbol{G})} \tag{14}$$

where $\boldsymbol{G}$ is a covariant metric tensor of the gradient of local element spatial coordinates $\xi$ with respect to the global coordinates $x$

$$\boldsymbol{G} = \left(\frac{\partial \boldsymbol{\xi}}{\partial \boldsymbol{x}}\right)^T \frac{\partial \boldsymbol{\xi}}{\partial \boldsymbol{x}}, \tag{15}$$

$\partial \boldsymbol{\xi} / \partial \boldsymbol{x}$ is the Jacobian matrix. $\boldsymbol{G} : \boldsymbol{G}$ denotes a double dot product of the two matrices, $c_1$, $c_2$ and $c_3$ are set to 4, 36 and 4 for the trilinear elements used in the present study. $tr(\boldsymbol{G})$ in Eq. (14) represents the trace of $\boldsymbol{G}$.

### 2.4. Time discretization

A generalized-$\alpha$ method [45] is employed to advance the discrete form of Eq. (10). Re-arranging the terms in Eq. (10) into the time derivative term and the other terms yields the following simple system

$$A(\boldsymbol{a})\dot{\boldsymbol{a}} = B(\boldsymbol{a})\boldsymbol{a}. \tag{16}$$

where $\boldsymbol{a}$ denotes the nodal values of $\{\boldsymbol{u}^h, p^h\}^T$, $\dot{\boldsymbol{a}}$ represents the temporal derivative of $\boldsymbol{a}$, $M$ and $N$, including nonlinear velocity terms, are matrices of $\dot{\boldsymbol{a}}$ and $\boldsymbol{a}$ respectively. Introducing the generalized-$\alpha$ method for the above nonlinear ordinary differential equation system yields

$$\boldsymbol{R}(\dot{\boldsymbol{a}}_{n+\alpha_m}, \boldsymbol{a}_{n+\alpha_f}) = A\dot{\boldsymbol{a}}_{n+\alpha_m} - B\boldsymbol{a}_{n+\alpha_f} = \boldsymbol{0}, \tag{17}$$

$$\boldsymbol{a}_{n+1} = \boldsymbol{a}_n + \Delta t \dot{\boldsymbol{a}}_n + \gamma \Delta t (\dot{\boldsymbol{a}}_{n+1} - \dot{\boldsymbol{a}}_n), \tag{18}$$

$$\dot{\boldsymbol{a}}_{n+\alpha_m} = \dot{\boldsymbol{a}}_n + \alpha_m (\dot{\boldsymbol{a}}_{n+1} - \dot{\boldsymbol{a}}_n), \tag{19}$$

$$\boldsymbol{a}_{n+\alpha_f} = \boldsymbol{a}_n + \alpha_f (\boldsymbol{a}_{n+1} - \boldsymbol{a}_n). \tag{20}$$

Parameters $\alpha_m$, $\alpha_f$ and $\gamma$ are selected based on considerations of accuracy and stability. It was deduced in [45] that second-order accuracy in time is attained if

$$\gamma = 0.5 + \alpha_m + \alpha_f, \tag{21}$$

and unconditional stability is achieved when

$$\alpha_m \geq \alpha_f \geq 1/2. \tag{22}$$

For strict control of high frequency damping, $\alpha_m$ and $\alpha_f$ are expressed in terms of the spectral radius $\zeta$ for an infinite time step,

$$\alpha_m = \frac{1}{2}\left(\frac{3-\zeta}{1+\zeta}\right), \quad \alpha_f = \frac{1}{1+\zeta}. \tag{23}$$

Here $\zeta$ is chosen to be 0.5.

A prediction-multicorrection iterative procedure is used to handle the generalized-algorithms (Eqs. (17)–(20)). With initial predictions of $\boldsymbol{a}$ and $\dot{\boldsymbol{a}}$, $\boldsymbol{a}_{n+\alpha_f}$ is corrected through $\Delta \boldsymbol{a}_{n+\alpha_f}$, which is obtained by solving a Newton's linearization system of $\boldsymbol{R}$ with respect to the solution variable. $\dot{\boldsymbol{a}}_{n+\alpha_m}$ is corrected through a function of $\boldsymbol{a}_{n+\alpha_f}$ obtained from Eqs. (18)–(20) by eliminating $\boldsymbol{a}_{n+1}$ and $\dot{\boldsymbol{a}}_{n+1}$. In the iterative procedure, $\boldsymbol{a}_{n+\alpha_f}$ and $\dot{\boldsymbol{a}}_{n+\alpha_m}$ are updated until $\Delta \boldsymbol{a}_{n+\alpha_f}$ is less than a given tolerance. The solutions at $t_{n+1}$ are then determined using Eqs. (19)–(20).

## 3. Resolved large-scale energy transportation equation

In the present method, the small scales are explicitly expressed based on the residual of the resolved-scale Navier–Stokes equations and only the large scales are numerically computed, thus the resolved-scale energy transportation

can be used to examine the energy evolution of the flow. In an arbitrary subdomain $\Omega_e \subset \Omega$, local kinetic energy of the large scales can be defined as $\int \frac{1}{2}\|\boldsymbol{u}^h\|^2 d\Omega_e = \frac{1}{2}(\boldsymbol{u}^h, \boldsymbol{u}^h)_{\Omega_e}$, where $\|\cdot\|^2$ denotes the standard $L^2$-norm and $\frac{1}{2}\|\boldsymbol{u}^h\|^2 = \frac{1}{2}\left((u_1^h)^2 + (u_2^h)^2 + (u_3^h)^2\right)$ represents the kinetic energy per unit volume. Therefore, the transportation equation of the kinetic energy per unit volume of the resolved large scales can be derived by taking $\boldsymbol{w}^h = \boldsymbol{u}^h$ in Eq. (10),

$$\begin{aligned}\frac{1}{2}d_t\|\boldsymbol{u}^h\|^2 = &-\boldsymbol{u}^h\cdot\nabla(\frac{1}{2}\|\boldsymbol{u}^h\|^2) + (\nabla\cdot\boldsymbol{u}^h)p^h - \nu\|\nabla\boldsymbol{u}^h\|^2 \\ &+ \underbrace{(\nabla\boldsymbol{u}^h):(\boldsymbol{u}^h\otimes\boldsymbol{u}')}_{(1)}\underbrace{-\boldsymbol{u}'\cdot\nabla(\frac{1}{2}\|\boldsymbol{u}^h\|^2)}_{(2)} + \underbrace{(\nabla\boldsymbol{u}^h):(\boldsymbol{u}'\otimes\boldsymbol{u}')}_{(3)} + \underbrace{(\nabla\cdot\boldsymbol{u}^h)p'}_{(4)} \\ &- \boldsymbol{u}^h\cdot\left(p^h\boldsymbol{n} - 2\nu\nabla^s\boldsymbol{u}^h\cdot\boldsymbol{n}\right)|_\Gamma + \boldsymbol{u}^h\cdot\boldsymbol{f},\end{aligned} \tag{24}$$

where $d_t$ represents the time derivative, $\boldsymbol{u}^h\cdot\nabla(\frac{1}{2}\|\boldsymbol{u}^h\|^2)$ is transport terms (also called kinetic energy flux) which transfer quantities from one region to another [46]. $\nu\|\nabla\boldsymbol{u}^h\|^2$ is rate of viscous dissipation of local kinetic energy. $(\nabla\cdot\boldsymbol{u}^h)p^h$ represents rate of the work by volume expansion, which is in principle zero due to incompressibility. $\boldsymbol{u}^h\cdot\boldsymbol{f}$ is rate of work by body force. $-\boldsymbol{u}^h\cdot\left(p^h\boldsymbol{n} - 2\nu\nabla^s\boldsymbol{u}^h\cdot\boldsymbol{n}\right)|_\Gamma$ is total rate of work by shear stress. The second line includes additional terms caused by the VMS method. According to the addressment in [1,2], these terms are constructed to account for the dynamical effect of the fine scales on the coarse-scale problem like the LES model. In the energy transportation process, they in principle transfer the kinetic energy from the resolved large scales to the unresolved small scales and complement the loss of dissipation due to the unresolved small scales.

## 4. Comparison with classical LES

### 4.1. SGS models for classical LES

As a reference for describing the present method, the classical LES by applying a filter to the Navier–Stokes equations is considered here for comparison. In the classical LES, both the widely-used Smagorinsky model and the Dynamic model from Germano identity are used for the subgrid-scale stress. The subgrid-scale stress is written as

$$T = 2\nu_T\tilde{S}_{ij}, \tag{25}$$

where $\tilde{S}_{ij} = \frac{1}{2}(\frac{\partial\tilde{u}_i}{\partial x_j} + \frac{\partial\tilde{u}_j}{\partial x_i})$ is the resolved large-scale strain rate tensor, $\nu_T$ denotes the subgrid-scale eddy viscosity and is defined as

$$\nu_T = (C_S^\Delta\tilde{\Delta})^2|\tilde{S}_{ij}|, \tag{26}$$

$C_S^\Delta$ is the model coefficient, $\tilde{\Delta}$ represents the filter width. For the Smagorinsky model, $C_S^\Delta$ is set to 0.1. In the dynamic SGS, $C_S^\Delta$ is dynamically adjusted to the local structure of the flow by an introduction of another filter width $\hat{\tilde{\Delta}}$. $C_S^\Delta$ is then computed from

$$(C_S^\Delta)^2 = \frac{\langle L_{ij}M_{ij}\rangle}{\langle M_{ij}M_{ij}\rangle}, \tag{27}$$

where

$$L_{ij} = \hat{\tilde{u}}_i\hat{\tilde{u}}_j - \widehat{\tilde{u}_i\tilde{u}_j} - \frac{1}{3}\left(\hat{\tilde{u}}_k\hat{\tilde{u}}_k - \widehat{\tilde{u}_k\tilde{u}_k}\right), \tag{28}$$

$$M_{ij} = 2\left(\hat{\tilde{\Delta}}^2|\hat{\tilde{S}}|\hat{\tilde{S}}_{ij} - \tilde{\Delta}^2\widehat{|\tilde{S}|\tilde{S}_{ij}}\right), \tag{29}$$

$\langle\cdot\rangle$ represents the spatial averaging in the homogeneous directions.

### 4.2. Results of turbulent channel flow at $Re_\tau = 180$

Benchmark turbulent channel flow at $Re_\tau = 180$ ($Re_\tau = u_\tau\delta/\nu$, $u_\tau = \sqrt{\tau/\rho}$ is friction velocity based on wall shear stress $\tau$ and fluid density $\rho$, $\delta$ is half the channel height), which is driven by a pressure gradient (body force $\boldsymbol{f} = \{1, 0, 0\}$) in the streamwise direction, is considered for numerical analysis of the present method.

**Table 1**
Computational parameters.

| $L_x \times L_y \times L_z$ | $N_x \times N_y \times N_z$ | $\alpha_s$ | $\Delta y^+_{min}$ |
|---|---|---|---|
| $2\pi \times 2 \times 4\pi/3$ | $32 \times 64 \times 32$ | 1.5 | 0.88 |

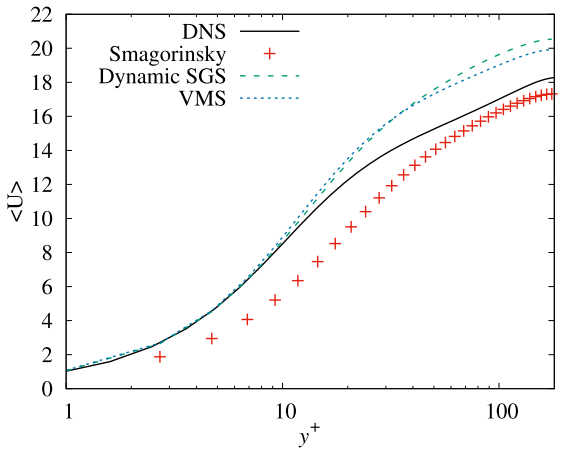


**Fig. 1.** Mean streamwise velocity $\langle U \rangle$ profiles of turbulent channel flow against $y^+$ at $Re_\tau = 180$.

Computational domain is a rectangular channel of $2\pi \times 2 \times 4\pi/3$. Simulations are performed using a mesh with $32 \times 64 \times 32$ trilinear hexahedral elements. A stretched mesh obtained by a two-sided hyperbolic tangent function is applied in the wall-normal direction,

$$y_j = 0.5 \left( \frac{\tanh\left(\alpha_s \left(\frac{2j}{N_y} - 1\right)\right)}{\tanh(\alpha_s)} + 1 \right), \tag{30}$$

where $N_y$ is the number of wall-normal nodes and $y_j$ is the wall-normal coordinate of the $j$th node. Detailed computational parameters are shown in Table 1. The same meshes are used for both the finite element method and finite difference method. The time step is set to 0.001.

The residual-based LES is implemented using in-house FEM codes developed by C++. A Newton–Raphson iterative procedure is used to solve the non-linear system of algebraic equations (17)–(20). The tangent matrix equation in each Newton–Raphson iteration is solved in parallel using a GMRES solver with a block ILU(0) preconditioning.

The classical LES is implemented using a finite difference method [47], in which a fractional-step method is employed to solve the filtered Navier–Stokes equations and spatial derivatives are discretized with a second-order central difference on a staggered grid. Time advancement is performed by the semi-implicit scheme mixing the Crank–Nicolson scheme for the viscous terms and the third-order Runge–Kutta scheme for the convective terms.

Numerical results are presented in the form of first- and second-order statistical quantities, including mean streamwise velocity, root-mean-square (RMS) profiles of velocity fluctuations in three directions and Reynolds stress. 10 000 snapshots of the fully-developed flow field in 50 nondimensional time units are used to compute the averaged quantities in both homogeneous directions and time. Fig. 1 shows the mean streamwise velocity profiles against the non-dimensional distance from the wall ($y^+ = u_\tau y/\nu$). For comparison, the DNS result obtained by Kim et al. [48] is plotted as well. As can be seen, the mean streamwise velocity is largely under-predicted by the classical LES with the Smagorinsky model, especially in the inner layer ($y/\delta < 0.1$). The results in the inner layer obtained by the classical LES with the dynamic SGS model and the present residual-based LES are in good agreement with the DNS data. Certain over-estimations are still caused in the outer layer ($y^+ < 50$) with using the present mesh. In contrast, the present LES results in better values of the mean streamwise velocity than the classical LES with the dynamic SGS models.

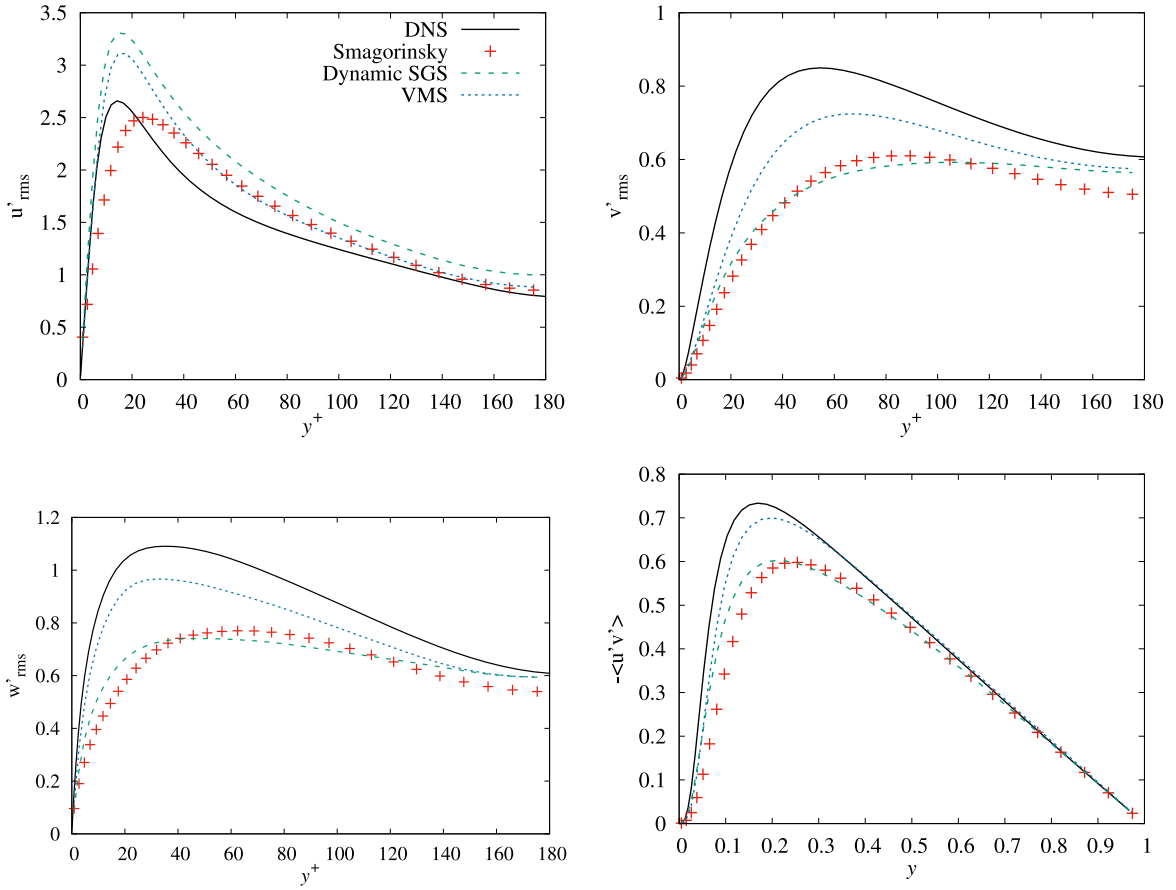


**Fig. 2.** Profiles of root-mean-square (RMS) magnitudes ($u'_{rms}$, $v'_{rms}$, $w'_{rms}$) of the velocity fluctuations and Reynolds stress ($-\langle u'v'\rangle$) of turbulent channel flow at $Re_\tau = 180$.

The profiles of the root-mean-square (RMS) magnitudes of the velocity fluctuations and Reynolds stress are shown in Fig. 2. In contrast to the DNS result, the RMS peak of the streamwise velocity fluctuations ($u'_{rms}$, the prime in all the statistical variables denotes fluctuations obtained by subtracting the mean from the solution) obtained by the classical LES with the Smagorinsky model is shifted to the higher $y^+$. The position of the $u'_{rms}$ peak obtained by the classical LES with the dynamic SGS model and the residual-based LES is at $y^+ \approx 15$, which is consistent with the DNS result. Obviously, the magnitude of $u'_{rms}$ obtained by the residual-based LES is in better agreement with the DNS data than that obtained by the classical LES with the dynamic SGS model. The RSM magnitudes of the normal ($v'_{rms}$) and spanwise ($w'_{rms}$) velocity fluctuations are quite under-estimated by the two classical LES, the present residual-based LES provides better profiles for ($v'_{rms}$) and ($w'_{rms}$). The reason can be found in the profiles of the Reynolds stress ($-\langle u'v'\rangle$). The residual-based LES makes better Reynolds stress ($-\langle u'v'\rangle$) prediction than the two classical LES, which strengthens the energy transportation from the streamwise velocity to the velocity fluctuations.

## 5. Turbulent kinetic dissipation analysis for the VMS method

It is well known that the additional terms (stabilized terms) involved with $\boldsymbol{u}'$ and $p'$ in the VMS method are introduced for the purpose of achieving a stable, consistent and convergent discretization. From the point of view of turbulent flow simulation, the stabilization terms and subgrid scale models in the classical LES pursue similar purposes. Both aims at representing the effect of unresolved small scales on resolved large scales by introducing proper dissipative mechanisms when bad discretization is encountered. However, the "proper dissipative

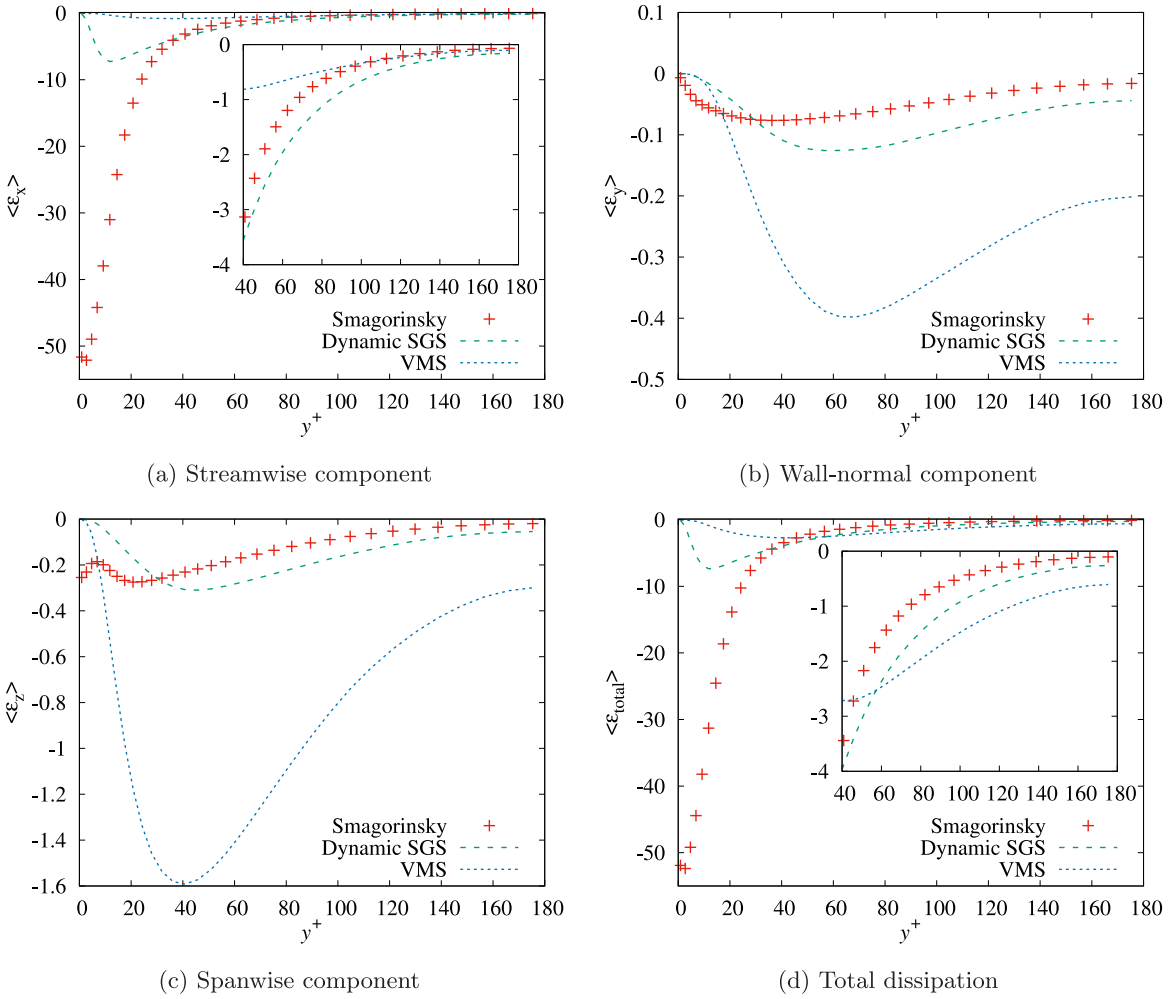


**Fig. 3.** Comparisons of the total numerical diffusion in the VMS method with the turbulent kinetic dissipation provided by the SGS model in the classical LES in the turbulent channel flow at $Re_\tau = 180$.

mechanisms" deserves special attention. To put insight into the numerical diffusion by the additional terms in the VMS method, we take the average of the summation of all the additional terms involved with $\boldsymbol{u}'$ and $p'$ in Eq. (24) (Terms (1), (2), (3) and (4)) over the homogeneous directions ($x$-axis and $z$-axis) and a certain time range ($T$),

$$\langle \epsilon_{total} \rangle = \frac{1}{L_x \times L_z \times T} \iiint ((\nabla \boldsymbol{u}^h) : (\boldsymbol{u}^h \otimes \boldsymbol{u}') - \boldsymbol{u}' \cdot \nabla(\frac{1}{2}\|\boldsymbol{u}^h\|^2) + (\nabla \boldsymbol{u}^h) : (\boldsymbol{u}' \otimes \boldsymbol{u}') + (\nabla \cdot \boldsymbol{u}^h)p')dxdzdt, \tag{31}$$

$\langle \epsilon_{total} \rangle$ can also be written in a tensor form as

$$\langle \epsilon_{total} \rangle = \frac{1}{L_x \times L_z \times T} \iiint (\frac{\partial u_i^h}{\partial x_j} u_j^h u_i' - u_i^h u_j' \frac{\partial u_i^h}{\partial x_j} + \frac{\partial u_i^h}{\partial x_j} u_j' u_i' + \frac{\partial u_i^h}{\partial x_i} p')dxdzdt. \tag{32}$$

For $i = 1, 2, 3$, it has three components corresponding to the streamwise ($\langle \epsilon_x \rangle$), wall-normal ($\langle \epsilon_y \rangle$) and spanwise ($\langle \epsilon_z \rangle$) direction respectively, $\langle \epsilon_{total} \rangle = \langle \epsilon_x \rangle + \langle \epsilon_y \rangle + \langle \epsilon_z \rangle$. Fig. 3 shows the profiles of $\langle \epsilon_x \rangle$, $\langle \epsilon_y \rangle$, $\langle \epsilon_z \rangle$ and $\langle \epsilon_{total} \rangle$ against $y^+$. Since the dissipation profiles are symmetric about the centreline of the channel, they are averaged using the data on the two sides and plotted just over the half channel. For comparison, profiles of the turbulent kinetic dissipation provided by the Smagorinsky and dynamic SGS model in the classical LES are also plotted in the

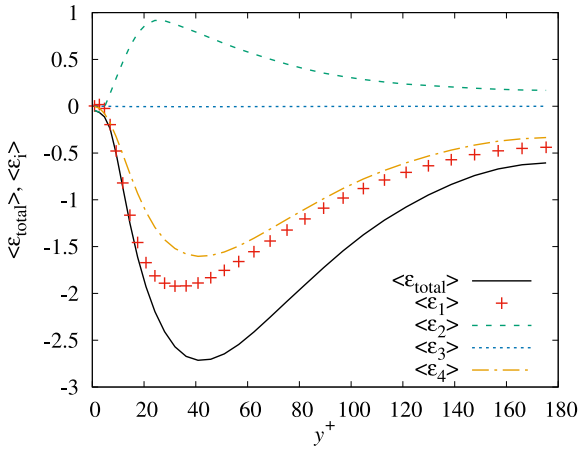


**Fig. 4.** Comparison of averaged magnitudes of Terms (1), (2), (3) and (4) in Eq. (24) against $y^+$ in the turbulent channel flow at $Re_\tau = 180$.

figure,

$$\langle \epsilon_{total} \rangle = \frac{1}{L_x \times L_z \times T} \iiint \left( -\nu_T \frac{\partial \bar{u}_i}{\partial x_j} \frac{\partial \bar{u}_i}{\partial x_j} \right) dxdzdt. \tag{33}$$

It can be seen that the Smagorinsky model engenders very high dissipation in the viscous sublayer ($y^+ < 5$). This could explain why the mean streamwise velocity and second-order statistics obtained by the LES with the Smagorinsky model is much under-predicted. The dynamic SGS model gives rise to lower dissipation in the inner layer, higher one in the outer layer than the Smagorinsky model. It is noted that the dissipation provided by the SGS model in the classical LES is mainly provided by its streamwise component. The numerical diffusions in the VMS method behave quite differently. Firstly, $\langle \epsilon_{total} \rangle$ is not dominated by the streamwise component, its three components are rather comparable. Secondly, the dissipation provided by the residual-based unresolved small scales in the VMS method is much smaller in the inner layer, larger in the outer region than that provided by the SGS model in the classical LES.

To clarify the contributions of the additional terms caused by the VMS method to the turbulent dissipations, we visit the average of Terms (1), (2), (3) and (4) in Eq. (24) separately,

$$\langle \epsilon_1 \rangle = \frac{1}{L_x \times L_z \times T} \iiint (\nabla \boldsymbol{u}^h) : (\boldsymbol{u}^h \otimes \boldsymbol{u}') dxdzdt, \tag{34}$$

$$\langle \epsilon_2 \rangle = \frac{1}{L_x \times L_z \times T} \iiint -\boldsymbol{u}' \cdot \nabla (\frac{1}{2} \|\boldsymbol{u}^h\|^2) dxdzdt, \tag{35}$$

$$\langle \epsilon_3 \rangle = \frac{1}{L_x \times L_z \times T} \iiint (\nabla \boldsymbol{u}^h) : (\boldsymbol{u}' \otimes \boldsymbol{u}') dxdzdt, \tag{36}$$

$$\langle \epsilon_4 \rangle = \frac{1}{L_x \times L_z \times T} \iiint (\nabla \cdot \boldsymbol{u}^h) p' dxdzdt. \tag{37}$$

Fig. 4 shows profiles of the averaged magnitudes of Terms (1), (2), (3) and (4) in Eq. (24) against $y^+$. Substituting the expression of $\boldsymbol{u}'$ into Term I, it becomes the same as the stabilization term in SUPG. The result shows that the value of $\langle \epsilon_1 \rangle$ is negative in the whole channel, suggesting an addition of the turbulent kinetic dissipation provided by Term I. Terms II and III only arise in the VMS method context. Fig. 4 shows that the value of $\langle \epsilon_2 \rangle$ is positive in the most part of the channel, which means that Term II does not dissipate the turbulent kinetic energy but increases energy with time in the resolved large-scale energy transportation equation. This actually differs from the intention of the turbulent model. In contrast with other terms, it can be seen that the value of $\langle \epsilon_3 \rangle$ is very small. For the negative value of $\langle \epsilon_3 \rangle$ in the most part of the channel (see the separated picture of $\langle \epsilon_3 \rangle$ in the next figure), it can be known that Term III provides dissipation in the resolved large-scale energy transportation equation. $p'$ in the VMS method is actually derived from the standard least-square stabilization for the incompressibility constraint [41,42].

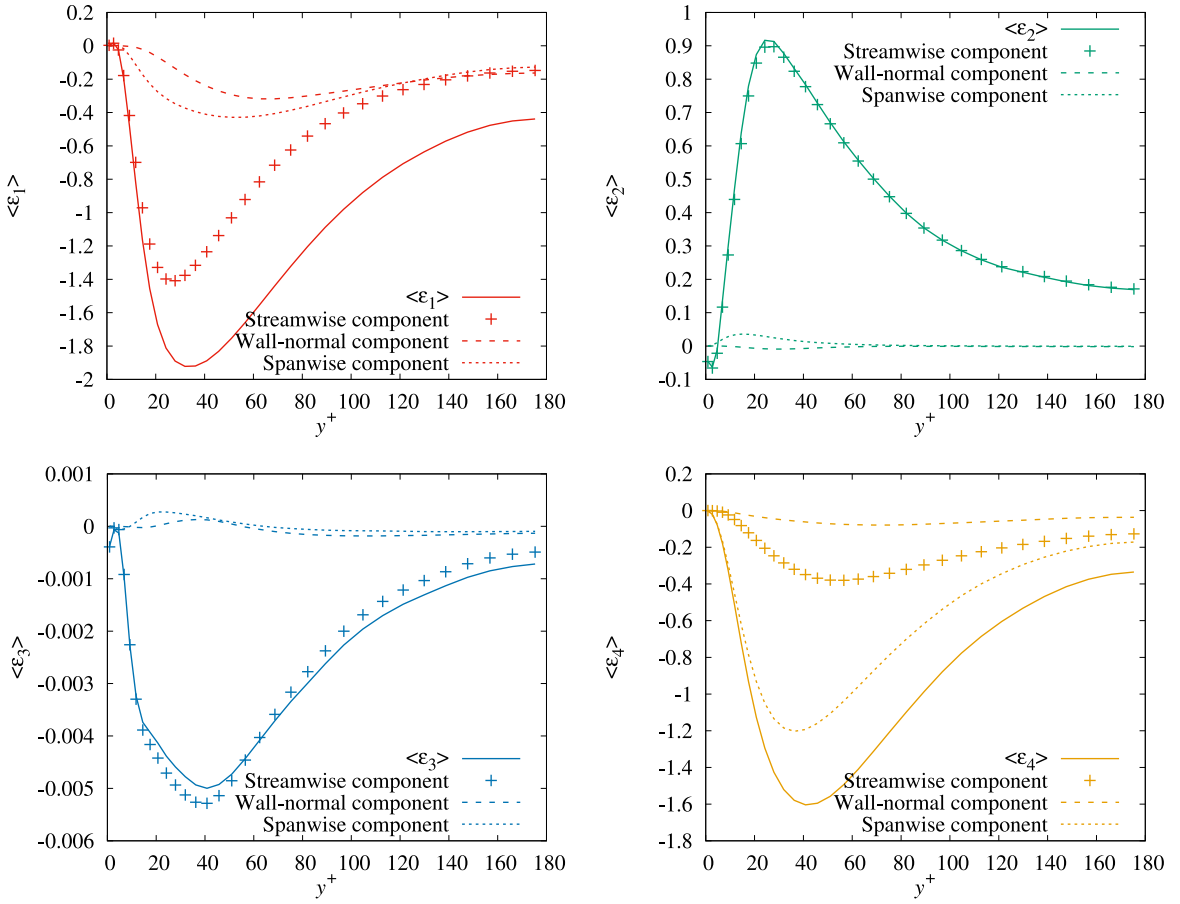


**Fig. 5.** Profiles of averaged magnitudes of Terms (1), (2), (3) and (4) in Eq. (24) and their three components against $y^+$ in the turbulent channel flow at $Re_\tau = 180$.

Therefore, Term IV is sometimes called LSIC term. According to the profile of $\langle\epsilon_4\rangle$, it is clear that the LSIC term also plays an important role in providing the additional dissipation.

Fig. 5 shows profiles of the averaged magnitude of each single term ($\langle\epsilon_1\rangle$, $\langle\epsilon_2\rangle$, $\langle\epsilon_3\rangle$ and $\langle\epsilon_4\rangle$) and its three components in Eq. (24). Substituting the expression of $\boldsymbol{u}'$ and taking the most dominant convection term of $\mathcal{L}(\boldsymbol{u}^h, p^h)$ in $\boldsymbol{u}'_i$ make Term I in Eq. (24) read as $-(\partial u_i^h/\partial x_j)u_j^h\tau_m u_k^h(\partial u_i^h/\partial x_k)$, which always stays negative when $j = k$. From the figure, it can be observed that the three components stay negative. Since the streamwise component of Term I includes the large gradient $\partial u_1^h/\partial x_2$, the streamwise component takes the most part of the $\langle\epsilon_1\rangle$. Similarly, taking the convection term of $\mathcal{L}(\boldsymbol{u}^h, p^h)$ in $\boldsymbol{u}'_j$, the dominant part of Term II in Eq. (24) can be written as $u_i^h\tau_m u_k^h(\partial u_j^h/\partial x_k)(\partial u_i^h/\partial x_j)$. The result shows that the streamwise component of Term II is positive in the most region of the channel (negative in $y^+ < 5$)and highly dominates the $\langle\epsilon_2\rangle$. The other two components are very small. The wall-normal component has an opposite sign with the streamwise and spanwise components in the most region. In the figure of $\langle\epsilon_3\rangle$, it is shown that Term III is negative in the most region of the channel and it is also highly dominated by its streamwise component. The other two components are very small and remain positive in a range of $10 < y^+ < 60$. Term IV reads as $-(\partial u_i^h/\partial x_i)\tau_c(\partial u_j^h/\partial x_j)$ by substituting the expression of $p'$. The profiles of $\langle\epsilon_4\rangle$ show that the spanwise component has the highest magnitude among three components of IV, the wall-normal component is relatively small.

According to the above analysis, the contribution of each additional term in the VMS method is made clear. Terms I, III and IV in Eq. (24) provide the turbulent dissipation in a way of numerical diffusion. Particularly, Term II is not able to supply the turbulent dissipation since it gives rise to the positive value of $\langle\epsilon_2\rangle$ in the resolved large-scale energy transportation equation.

## 6. A new stabilized finite element formulation

Adding extra subgrid dissipation in the presence of numerical dissipation has succeeded in the previous work, e.g. Martinez and Jansen have coupled the physical SGS model with SUPG method [49]. According to the dissipation analysis for the VMS method, neglecting Terms II may remove the positive part of $\langle \epsilon_{total} \rangle$ so as to increase the total numerical diffusion. Over such an inspiration, a new stabilized finite element formulation is proposed by modifying the large-scale equation of the variational multiscale formulation for the incompressible Navier–Stokes equations,

$$
\begin{aligned}
&\left(\boldsymbol{w}^h, \frac{\partial \boldsymbol{u}^h}{\partial t}\right)_{\Omega} + (\boldsymbol{w}^h, \boldsymbol{u}^h \cdot \nabla \boldsymbol{u}^h)_{\Omega} - (\nabla \boldsymbol{w}^h, p^h)_{\Omega} + \left(\nabla^s \boldsymbol{w}^h, 2\nu \nabla^s \boldsymbol{u}^h\right)_{\Omega} + (q^h, \nabla \cdot \boldsymbol{u}^h)_{\Omega} \\
&+ \underbrace{\sum_{e=1}^{n_{el}} \left(\boldsymbol{u}^h \cdot \nabla \boldsymbol{w}^h, \tau_m \boldsymbol{r}_m\right)_{\Omega_e}}_{①} + \underbrace{\sum_{e=1}^{n_{el}} \left(\boldsymbol{w}^h, \tau_m \boldsymbol{r}_m \cdot \nabla \boldsymbol{u}^h\right)_{\Omega_e}}_{②} - \underbrace{\sum_{e=1}^{n_{el}} \left(\nabla \boldsymbol{w}^h, \tau_m \boldsymbol{r}_m \otimes \tau_m \boldsymbol{r}_m\right)_{\Omega_e}}_{③} \\
&+ \underbrace{\sum_{e=1}^{n_{el}} \left(\nabla \cdot \boldsymbol{w}^h, \tau_c \nabla \cdot \boldsymbol{w}^h\right)_{\Omega_e}}_{④} \\
&+ \underbrace{\sum_{e=1}^{n_{el}} \left(\nabla q^h, \tau_m \boldsymbol{r}_m\right)_{\Omega_e}}_{⑤} \\
&+ \sum_{e=1}^{n_{eb}} \left(\boldsymbol{w}^h, p^h \boldsymbol{n} - 2\nu \nabla^s \boldsymbol{u}^h \cdot \boldsymbol{n}\right)_{\Gamma_e} \\
&= (\boldsymbol{w}^h, \boldsymbol{f})_{\Omega},
\end{aligned}
\tag{38}
$$

where $\tau_m$ and $\tau_c$ are the same as used in the VMS method. In the new stabilized finite element formulation, Terms (Terms ①, ③, ④ and ⑤) remain the same as Terms I, III, IV and V in Eq. (10), Term ② takes the same form but has an opposite sign with Term II in Eq. (10). The modelling terms are based on the large scale residual, and retain numerical consistency as well.

### 6.1. Test case 1: 2D lid-driven cavity flow

2D lid driven cavity steady flows are firstly tested for the new stabilized finite element formulation. The governing equations for the cavity flows are Eqs. (1) and (2) with $\boldsymbol{f} = \boldsymbol{0}$. Here two cases with $Re = 1000$ and 125 000 are tested. Two coarse meshes with $32 \times 32$ and $64 \times 64$ cells are respectively used for the simulations of the flows at $Re = 1000$ and 125 000.

Figs. 6(a) and 6(b) show the vertical velocity profiles along the horizontal geometric centre line and the horizontal velocity profiles along the vertical geometric centre line of the cavity at $Re = 1000$ and 125 000 respectively. The DNS results computed by Erturk et al. [50] are attached as a reference, the results by the VMS, SUPG and new stabilized method (it is also called 'modified VMS method' here) are compared. The results show that the velocity profiles are very close to each other at $Re = 1000$. When $Re$ increases to a higher value 125 000, the deviations among the velocity profiles by the three methods become visually clear. Through the zoom-in pictures of the high velocity gradient regions, it can be clearly seen that the VMS method does not show an advantage in comparison with the SUPG method. The newly proposed stabilized method makes the velocity profiles closer to the DNS results, especially the velocities at the nodes next to the wall.

### 6.2. Test case 2: 3D turbulent channel flow

The newly proposed stabilized finite element formulations are also tested in the benchmark turbulent channel flow at $Re_\tau = 180$. In the tests, the same computational parameters as adopted in Section 4.2 are used for the

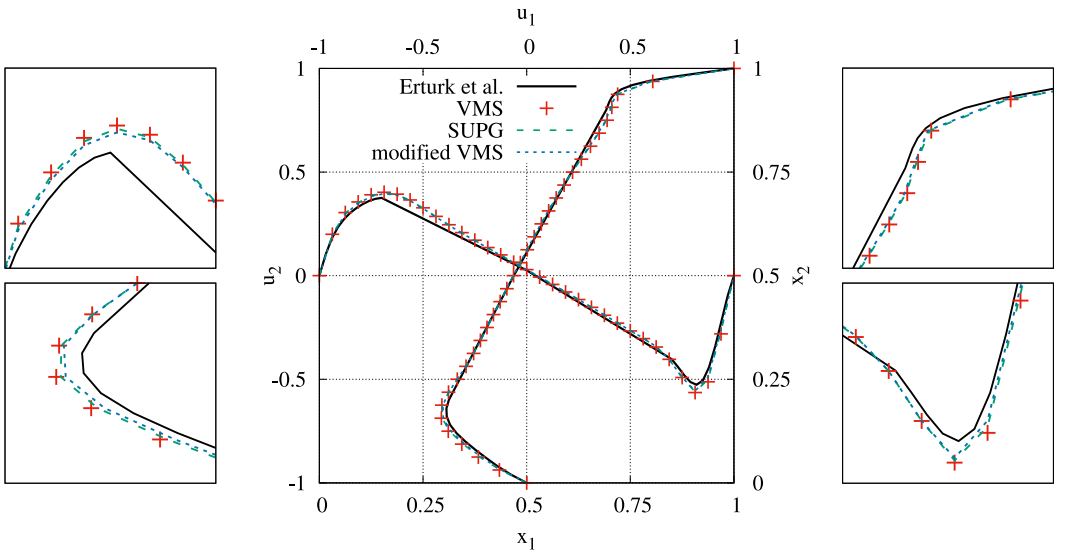


(a) $Re = 1000$

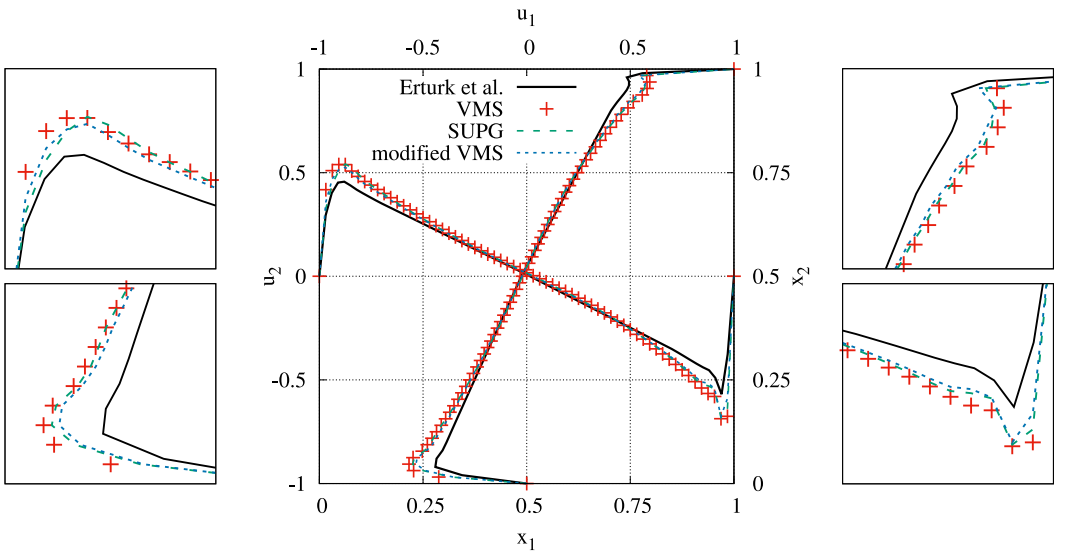


(b) $Re = 12500$

**Fig. 6.** Vertical velocity ($u_2$) profiles along the horizontal geometric centre line ($x_1$) and horizontal velocity ($u_1$) profiles along the vertical geometric centre line ($x_2$) of the cavity.

computations by the SUPG and new stabilized methods. Fig. 7 shows the first-order (mean streamwise velocity $\langle U \rangle$) and second-order (root-mean-square of the velocity fluctuations $u'_{rms}$, $v'_{rms}$, $w'_{rms}$ and Reynolds stress $-\langle u'v' \rangle$) statistical quantities against the normal distance from the wall. It is shown that the mean streamwise velocities obtained by the three methods are quite close to each other in the viscous sublayer ($y^+ < 10$). In the outer layer, the mean streamwise velocity obtained by the SUPG method is slightly closer to the DNS profile than that obtained by the VMS method. In contrast with the VMS and SUPG method, an improvement made by the newly proposed stabilized method can be clearly seen in the outer layer.

For the second-order statistical quantities, the SUPG and new stabilized methods make an apparent improvement in the profile of $u'_{rms}$ in the buffer layer ($5 < y^+ < 30$), and the new stabilized method results in the best $u'_{rms}$. The profiles of $v'_{rms}$ obtained by the three methods are quite similar. For the profile of $w'_{rms}$, the VMS and SUPG

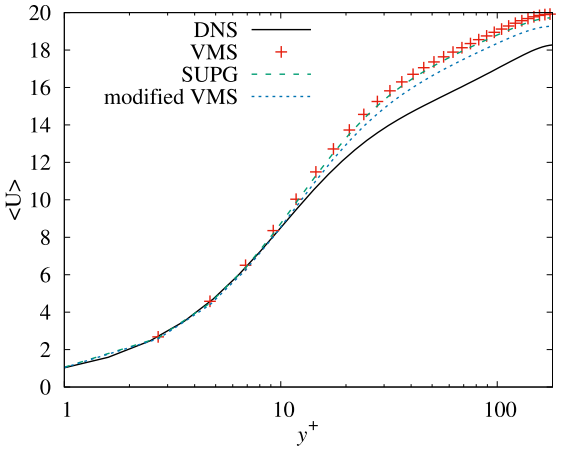


(a) Mean velocity.

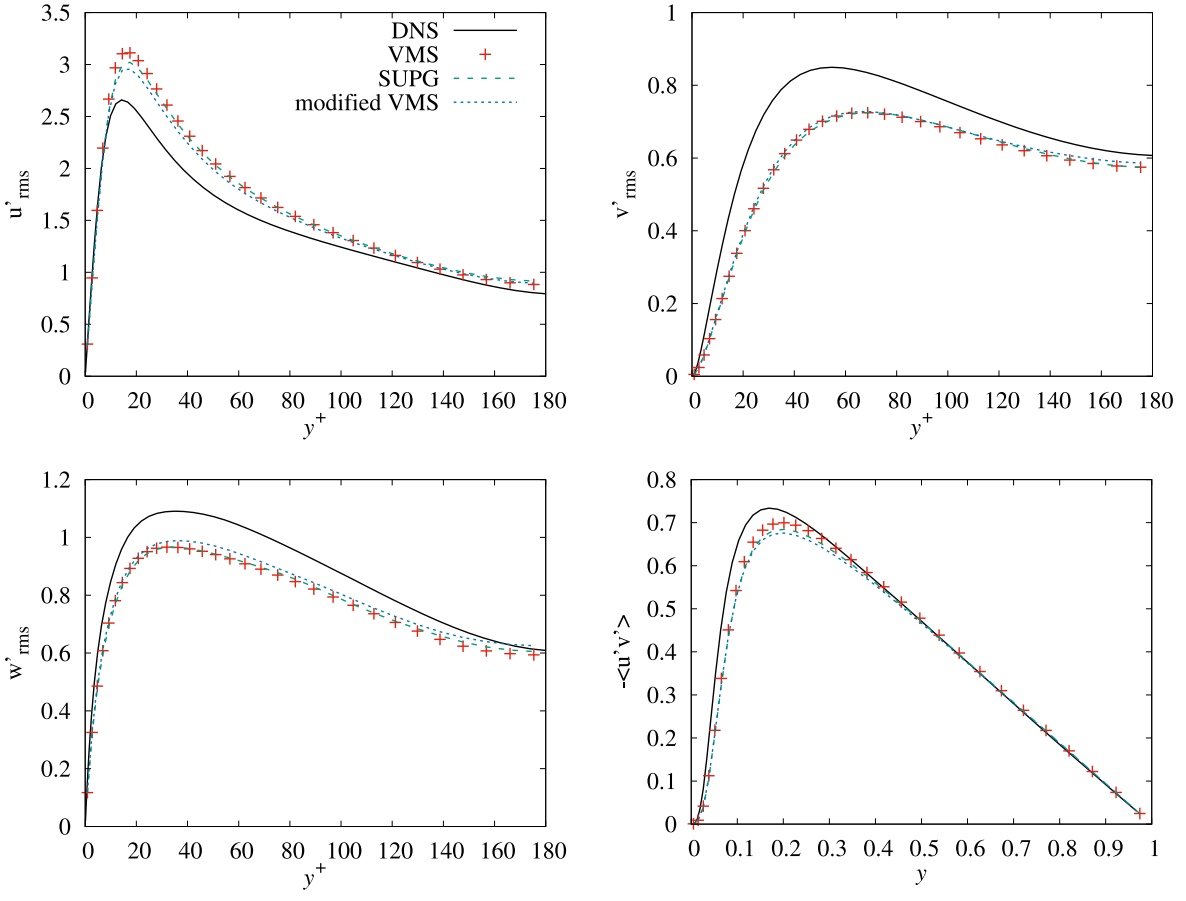


(b) $u'_{rms}$, $v'_{rms}$, $w'_{rms}$ and $< u'v' >$.

**Fig. 7.** Profiles of mean streamwise velocity ($\langle U \rangle$), root-mean-square (RMS) of the velocity fluctuations ($u'_{rms}$, $v'_{rms}$, $w'_{rms}$) against $y^+$ and Reynolds stress ($-\langle u'v' \rangle$) against $y$.

methods give rise to the very similar results, a small improvement is made in the outer layer by the new stabilized method. Besides, in comparison with the VMS method, the Reynolds stress $-\langle u'v'\rangle$ produced by the SUPG and new stabilized methods slightly decreases.

Replacing $\boldsymbol{w}^h$ with $\boldsymbol{u}^h$ and taking an inner product of each term in Eq. (38) yields the energy transportation equation of the newly proposed stabilized finite element formulation,

$$\begin{aligned}\frac{1}{2}d_t\|\boldsymbol{u}^h\|^2 = &-\boldsymbol{u}^h\cdot\nabla(\frac{1}{2}\|\boldsymbol{u}^h\|^2)+(\nabla\cdot\boldsymbol{u}^h)p^h-\nu\|\nabla\boldsymbol{u}^h\|^2\\ &\underbrace{-(\boldsymbol{u}^h\cdot\nabla\boldsymbol{u}^h)\cdot(\tau_m\boldsymbol{r}_m)}_{(1)}\underbrace{-\tau_m\boldsymbol{r}_m\cdot\nabla(\frac{1}{2}\|\boldsymbol{u}^h\|^2)}_{(2)}+\underbrace{(\nabla\boldsymbol{u}^h):(\tau_m\boldsymbol{r}_m\otimes\tau_m\boldsymbol{r}_m)}_{(3)}\underbrace{-(\nabla\cdot\boldsymbol{u}^h)\tau_c(\nabla\cdot\boldsymbol{u}^h)}_{(4)}\\ &-\boldsymbol{u}^h\cdot\left(p^h\boldsymbol{n}-2\nu\nabla^s\boldsymbol{u}^h\cdot\boldsymbol{n}\right)|_\Gamma+\boldsymbol{u}^h\cdot\boldsymbol{f},\end{aligned}\tag{39}$$

Profiles of the dissipations provided by the additional terms in the three methods are shown in Fig. 8. In the SUPG method, only Terms (1) and (4) are considered. In Fig. 8(a), it can be seen that the total numerical diffusion provided by the SUPG method is larger than that provided by the VMS method as Terms II and III in Eq. (10) are neglected. In the new stabilized method, owing to the replacement of Term II in Eq. (10) with Term ① in Eq. (38), the total numerical diffusion substantially increases, and it is even larger than that provided by the SUPG method. Physically, the larger numerical diffusion implies the higher turbulent kinetic dissipation, it dissipates the bulk velocity and allows the mean velocity profile to become closer to the solution when using a coarse mesh. This is why an improvement in the mean streamwise profile is obtained by the new stabilized method in Fig. 7(a). The larger numerical diffusion may also alleviate the numerical perturbations in the convection-dominated direction. This causes that the profile of $u'_{rms}$ becomes better when the new stabilized method is used. For the nonlinearity of the residual-based stabilization terms in the stabilized method, the $w'_{rms}$ does not decrease but increase somehow.

In the profiles of each single term in Fig. 8(b), it can be observed that, in comparison with the VMS method, the present stabilized method does not cause a distinct change of the numerical diffusions provided by Terms ①, ③ and ④. The $\langle\epsilon_1\rangle$, $\langle\epsilon_3\rangle$ and $\langle\epsilon_4\rangle$ provided by the new stabilized method are similar to those provided by both the VMS and SUPG methods. The $\langle\epsilon_2\rangle$ produced by the present stabilized method has opposite sign with the one produced by the VMS method, which mainly leads to increase of the numerical diffusion in the new stabilized method. Owing to the nonlinearity of the addition numerical diffusion terms, small decreases of the $\langle\epsilon_1\rangle$, $\langle\epsilon_3\rangle$ and $\langle\epsilon_4\rangle$ are triggered and the $\langle\epsilon_2\rangle$ profile by the new stabilized method is not completely symmetric with that by the VMS method about the axis $\langle\epsilon_2\rangle = 0$.

In particular, not only does the proposed stabilized formulation improves the statistical results, its numerical consistency also ensures that the numerical diffusion provided by the modelling terms dynamically reduces with refinement until it vanishes when grid spacing satisfies DNS. These properties guarantee validity of the method in other meshes.

## 7. Conclusions

The residual-based large eddy simulation by the variational multiscale method is interpreted as an implicit LES, in which purely numerical diffusion terms replace the SGS model of the classical LES. The resolved large-scale energy transportation equations are mathematically derived for turbulent kinetic dissipation analysis. Statistical results of turbulent channel flow at $Re_\tau = 180$, including mean streamwise velocity, RMS of the velocity fluctuations and Reynolds stress obtained using a coarse mesh are compared with the results obtained by the classical LES with the Smagorinsky and dynamic SGS model. The present LES shows an advantage in predicting the statistical results of the incompressible turbulent flows, especially for the second-order statistical quantities.

Particularly, the contributions of the unresolved small-scale presentation terms to the turbulent kinetic dissipation are analysed for the VMS method in the study. It is found that the total turbulent kinetic dissipation provided by the numerical diffusion in the VMS method is smaller in the inner layer, larger in the outer layer of the channel flow than those by the Smagorinsky and dynamic SGS model. The total turbulent kinetic dissipation in the VMS method is mainly given by the numerical diffusion provided by one of the "cross-stress" terms (Term I, same as the stabilization term in the SUPG method) and LSIC term (Term IV) in the variational multiscale formulation. The other one of the "cross-stress" terms (Term II) gives rise to the positive turbulent kinetic energy budget, and

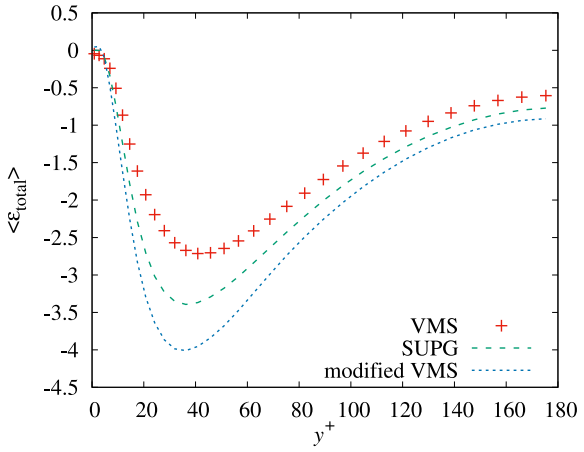


(a) Total dissipation.

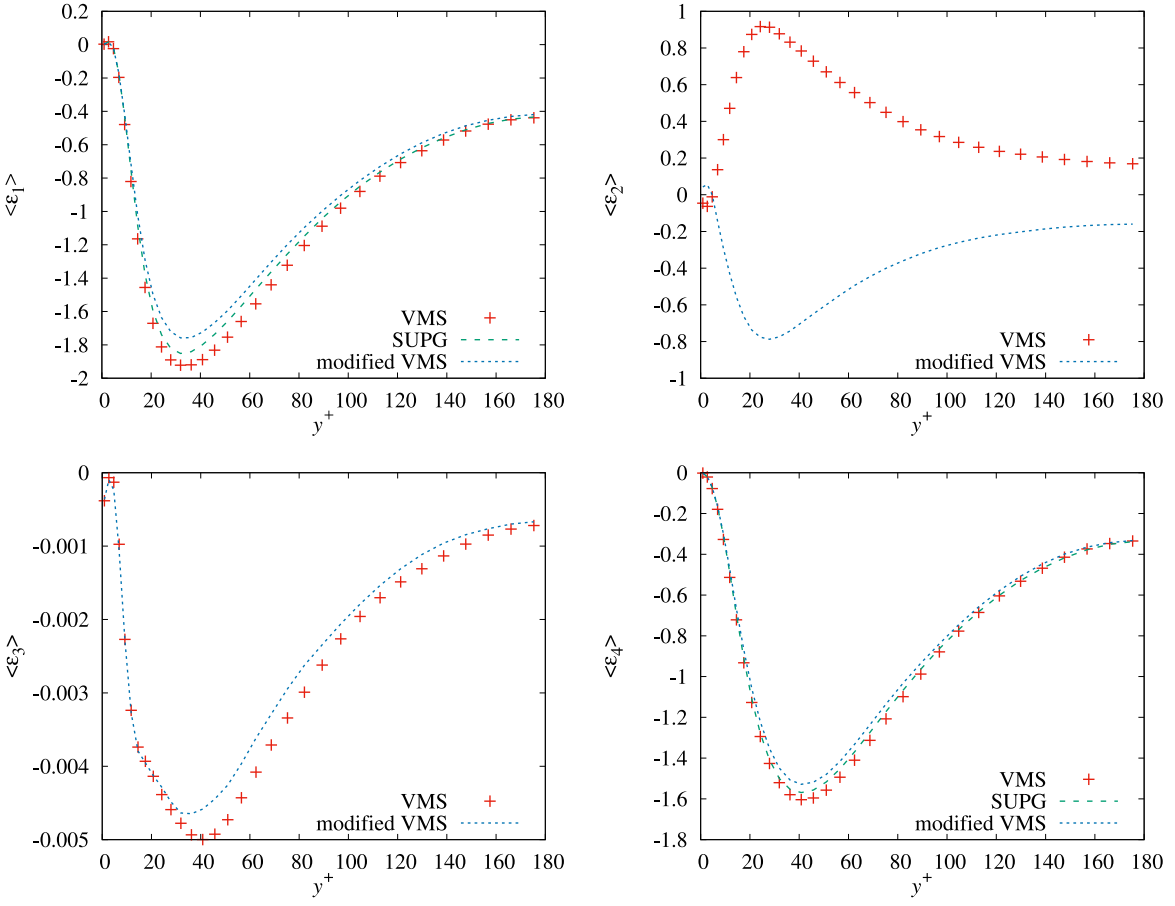


(b) Kinetic energy budget by each single term.

**Fig. 8.** Turbulent kinetic energy budget profiles provided by the additional numerical diffusion terms in the VMS, SUPG and new stabilized finite element formulation at $Re_\tau = 180$.

does not dissipate the turbulent kinetic energy. The so-called "Reynolds stress" term (Term III) in the variational multiscale formulation dissipates the turbulent energy but provides a very small numerical diffusion.

On the basis of the turbulent kinetic energy dissipation analysis for the VMS method, a new residual-based stabilized finite element formulation is proposed by modifying the large-scale equation in the VMS method. Numerical experiments of 2D lid-driven cavity flow and 3D benchmark turbulent channel flow are tested to validate the proposed formulation. According to the results, all the stabilization terms in the proposed formulation produce additional numerical diffusions and physically increase the total turbulent kinetic dissipation. Therefore, an apparent improvement in both the first-order and second-order statistical quantities are pursued. In addition, the numerical consistency ensures that the numerical diffusions provided by the stabilization terms dynamically reduces with refinement until it vanishes when griding space satisfies DNS, guaranteeing validity of the proposed formulation in other meshes.

## Declaration of competing interest

The authors declare that they have no known competing financial interests or personal relationships that could have appeared to influence the work reported in this paper.

## Acknowledgements

The authors wish to express their appreciation for the support provided by the Natural Science Foundation of Jiangsu Province (BK20180981), and the National Natural Science Foundation of China (Grant No. 12172207, 91852111, 51879123).

## References

[1] V. Calo, Residual-based multiscale turbulence modeling: Finite volume simulations of bypass transition, (Ph.D. thesis), Stanford University, Stanford, CA, USA, 2005.
[2] Y. Bazilevs, V.M. Calo, J.A. Cottrell, T.J.R. Hughes, A. Reali, G. Scovazzi, Variational multiscale residual-based turbulence modeling for large eddy simulation of incompressible flows, Comput. Methods Appl. Mech. Engrg. 197 (1–4) (2007) 173–201.
[3] T.J.R. Hughes, L. Mazzei, K.E. Jansen, Large eddy simulation and the variational multiscale method, Comput. Vis. Sci. 3 (2000) 47–59.
[4] T.J.R. Hughes, Multiscale phenomena: Green's functions, the Dirichlet-to-Neumann formulation, subgrid scale models, bubbles and the origins of stabilized methods, Comput. Methods Appl. Mech. Engrg. 127 (1–4) (1995) 387–401.
[5] I. Akkerman, Adaptive variational multiscale formulations using the discrete germano approach, (Ph.D. thesis), Delft University of Technology, 2009.
[6] P. Sagaut, Large Eddy Simulation for Incompressible Flows, Springer Berlin Heidelberg, 2006.
[7] T.J.R. Hughes, G. Feijoo, L. Mazzei, J. Quincy, The variational multiscale method - a paradigm for computational mechanics, Comput. Methods Appl. Mech. Engrg. 166 (1–2) (1998) 3–24.
[8] T.J.R. Hughes, L. Mazzei, A.A. Oberai, A.A. Wray, The multiscale formulation of large eddy simulation: Decay of homogeneous isotropic turbulence, Phys. Fluids 13 (2) (2001) 505–512.
[9] T.J.R. Hughes, A.A. Oberai, L. Mazzei, Large eddy simulation of turbulent channel flows by the variational multiscale method, Phys. Fluids 13 (6) (2001) 1784–1799.
[10] V. John, Finite Element Methods for Incompressible Flow Problems, vol. 51, Springer, 2016.
[11] N. Ahmed, T.C. Rebollo, V. John, S. Rubino, A review of variational multiscale methods for the simulation of turbulent incompressible flows, Arch. Comput. Methods Eng. 24 (2017) 115–164.
[12] T.J.R. Hughes, J.A. Cottrell, Y. Bazilevs, Isogeometric analysis: CAD, finite elements, NURBS, exact geometry and mesh refinement, Comput. Methods Appl. Mech. Engrg. 194 (39–41) (2005) 4135–4195.
[13] Y. Bazilevs, C. Michler, V.M. Calo, T.J.R. Hughes, Isogeometric variational multiscale modeling of wall-bounded turbulent flows with weakly enforced boundary conditions on unstretched meshes, Comput. Methods Appl. Mech. Engrg. 199 (13–16) (2010) 780–790.
[14] Y. Bazilevs, I. Akkerman, Large eddy simulation of turbulent Taylor-Couette flow using isogeometric analysis and the residual-based variational multiscale method, J. Comput. Phys. 229 (9) (2010) 3402–3414.
[15] G. Motlagh, Yousef, Ahn, H. Taek, Hughes, J.R. Thomas, M. Victor, Simulation of laminar and turbulent concentric pipe flows with the isogeometric variational multiscale method, Comput. & Fluids 71 (2) (2013) 146–155.
[16] G. Bauer, P. Gamnitzer, V. Gravemeier, W.A. Wall, An isogeometric variational multiscale method for large-eddy simulation of coupled multi-ion transport in turbulent flow, J. Comput. Phys. 251 (4) (2013) 194–208.
[17] J.P. Trelles, S.M. Modirkhazeni, Variational multiscale method for nonequilibrium plasma flows, Comput. Methods Appl. Mech. Engrg. 282 (2014) 87–131.
[18] S. Riber, R. Valette, Y. Mesri, E. Hachem, Adaptive variational multiscale method for bingham flows, Comput. & Fluids 138 (2016) 51–60.
[19] L.F. Chen, G.X. Wu, Boundary shear flow past a cylinder near a wall, Appl. Ocean Res. 92 (2019) 101923.
[20] L.F. Chen, S.J. Hulshoff, Y.T. Wang, 2D residual-based LES of flow around a pipeline close to a flat seabed, Comput. Methods Appl. Mech. Engrg. 363 (2020) 112788.

[21] L. Chen, Y. Wang, S. Sun, S. Wang, The effect of boundary shear flow on hydrodynamic forces of a pipeline over a fully scoured seabed, Ocean Engineering 206 (2020) 107326.
[22] V. Gravemeier, W.A. Wall, Variational multiscale methods for premixed combustion based on a progress-variable approach, Combust. Flame 158 (6) (2011) 1160–1170.
[23] M. Khalloufi, Y. Mesri, R. Valette, E. Massoni, E. Hachem, High fidelity anisotropic adaptive variational multiscale method for multiphase flows with surface tension, Comput. Methods Appl. Mech. Engrg. 307 (2016) 44–67.
[24] U. Rasthofer, W.A. Wall, V. Gravemeier, An extended algebraic variational multiscale-multigrid-multifractal method (XAVM$^4$) for large-eddy simulation of turbulent two-phase flow, J. Comput. Phys. 359 (2018) 1–19.
[25] J. Yan, S. Lin, Y. Bazilevs, G.J. Wagner, Isogeometric analysis of multi-phase flows with surface tension and with application to dynamics of rising bubbles, Comput. & Fluids (2019) 777–789.
[26] I. Akkerman, Y. Bazilevs, C.E. Kees, M.W. Farthing, Isogeometric analysis of free-surface flow, J. Comput. Phys. 230 (11) (2011) 4137–4152.
[27] I. Akkerman, J. Dunaway, J. Kvandal, J. Spinks, Y. Bazilevs, Toward free-surface modeling of planing vessels: simulation of the fridsma hull using ALE-VMS, Comput. Mech. 50 (6) (2012) 719–727.
[28] I. Akkerman, Y. Bazilevs, D.J. Benson, M.W. Farthingc, C.E. Kees, Free-surface flow and fluid-object interaction modeling with emphasis on ship hydrodynamics, J. Appl. Mech. 79 (2012) 010905.
[29] J. Yan, X. Deng, A. Korobenko, Y. Bazilevs, Free-surface flow modeling and simulation of horizontal-axis tidal-stream turbines, Comput. & Fluids (2017) 157–166.
[30] L. Zhu, S.A. Goraya, A. Masud, Interface-capturing method for free-surface plunging and breaking waves, J. Eng. Mech. 145 (11) (2019) 04019088.
[31] L. Zhu, A. Masud, Variationally derived interface stabilization for discrete multiphase flows and relation with the ghost-penalty method, Comput. Methods Appl. Mech. Engrg. 373 (2021) 113404.
[32] J. Yan, A. Korobenko, A.E. Tejada-Martínez, R. Golshan, Y. Bazilevs, A new variational multiscale formulation for stratified incompressible turbulent flows, Comput. & Fluids 158 (2016) 150–156.
[33] I. Akkerman, Y. Bazilevs, V.M. Calo, T.J.R. Hughes, S. Hulshoff, The role of continuity in residual-based variational multiscale modeling of turbulence, Comput. Mech. 41 (3) (2008) 371–378.
[34] Z. Wang, A.A. Oberai, Spectral analysis of the dissipation of the residual-based variational multiscale method, Comput. Methods Appl. Mech. Engrg. 199 (13–16) (2010) 810–818.
[35] J. Principe, R. Codina, F. Henke, The dissipative structure of variational multiscale methods for incompressible flows, Comput. Methods Appl. Mech. Engrg. 199 (13–16) (2010) 791–801.
[36] O. Colomes, S. Badia, R. Codina, J. Principe, Assessment of variational multiscale models for the large eddy simulation of turbulent incompressible flows, Comput. Methods Appl. Mech. Engrg. 285 (2015) 32–63.
[37] M.F.P.T. Eikelder, I. Akkerman, Correct energy evolution of stabilized formulations: The relation between VMS, SUPG and GLS via dynamic orthogonal small-scales and isogeometric analysis. I: The convective-diffusive context, Comput. Methods Appl. Mech. Engrg. 331 (2018) 259–280.
[38] M.F.P.T. Eikelder, I. Akkerman, Correct energy evolution of stabilized formulations: The relation between VMS, SUPG and GLS via dynamic orthogonal small-scales and isogeometric analysis. II: The incompressible Navier-Stokes equations, Comput. Methods Appl. Mech. Engrg. 340 (2018) 1135–1154.
[39] N. Ahmed, S. Rubino, Numerical comparisons of finite element stabilized methods for a 2D vortex dynamics simulation at high Reynolds number, Comput. Methods Appl. Mech. Engrg. 349 (2019) 191–212.
[40] N. Ahmed, V. John, An assessment of two classes of variational multiscale methods for the simulation of incompressible turbulent flows, Comput. Methods Appl. Mech. Engrg. 365 (2020) 112997.
[41] L.P. Franca, S.L. Frey, Stabilized finite element methods: II. The incompressible Navier-Stokes equations, Comput. Methods Appl. Mech. Engrg. 99 (2–3) (1992) 209–233.
[42] M.A. Behr, L.P. Franca, T.E. Tezduyar, Stabilized finite element methods for the velocity-pressure-stress formulation of incompressible flows, Comput. Methods Appl. Mech. Engrg. 104 (1) (1993) 31–48.
[43] F. Shakib, Finite element analysis of the compressible Euler and Navier-Stokes equations, (Ph.D. thesis), Stanford, 1989.
[44] C.A. Taylor, T.J.R. Hughes, C.K. Zarins, Finite element modeling of blood flow in arteries, Comput. Methods Appl. Mech. Engrg. 158 (158) (1998) 155–196.
[45] K.E. Jansen, C.H. Whiting, G.M. Hulbert, A generalized-alpha method for integrating the filtered Navier-Stokes equations with a stabilized finite element method, Comput. Methods Appl. Mech. Engrg. 190 (3–4) (2000) 305–319.
[46] P.K. Kundu, I.M. Cohen, D.R. Dowling, Fluid Mechanics: Sixth Edition, 2015.
[47] Y.H. Dong, L.F. Chen, The effect of stable stratification and thermophoresis on fine particle deposition in a bounded turbulent flow, Int. J. Heat Mass Transfer 54 (5–6) (2011) 1168–1178.
[48] J. Kim, P. Moin, R. Moser, Turbulence statistics in fully developed channel flow at low Reynolds number, J. Fluid Mech. 177 (1987) 133–166.
[49] A.E. Tejada-Martinez, K.E. Jansen, On the interaction between dynamic model dissipation and numerical dissipation due to streamline upwind/Petrov-Galerkin stabilization, Comput. Methods Appl. Mech. Engrg. 194 (2005) 1225–1248.
[50] E. Erturk, T.C. Corke, C. Gokcol, Numerical solutions of 2-D steady incompressible driven cavity flow at high Reynolds numbers, Internat. J. Numer. Methods Fluids 48 (7) (2005) 747–774.